

# Microspectrofluorometry by Digital Image Processing: Measurement of Cytoplasmic pH

LERSON TANASUGARN, PAUL McNEIL, G. T. REYNOLDS,\* and D. LANSING TAYLOR  
*Center for Fluorescence Research in Biomedical Sciences, Department of Biological Sciences, Carnegie-Mellon University, Pittsburgh, Pennsylvania 15213; and \*Physics Department, Princeton University, Princeton, New Jersey 08544*

**ABSTRACT** An interface of our microspectrofluorometer with an image processing system performs microspectrofluorometric measurements in living cells by digital image processing. Fluorescence spectroscopic parameters can be measured by digital image processing directly from microscopic images of cells, and are automatically normalized for pathlength and accessible volume. Thus, an accurate cytoplasmic "map" of various spectroscopic parameters can be produced. The resting cytoplasmic pH of fibroblasts (3T3 cells) has been determined by measuring the ratio of fluorescein fluorescence excited by two successive wavelengths (489 and 452 nm). Fluorescein-labeled dextran microinjected into the cells is used as a pH indicator, since it is trapped in the cytoplasm but is excluded from the nucleus and other organelles. The average cytoplasmic pH is 6.83 ( $\pm$  0.38). However, cytoplasmic pH exhibits a non-unimodal distribution, the lower mean pH being 6.74 ( $\pm$  0.23). When 3T3 cells pinocytose medium containing fluorescein dextran, pinosomes peripheral to the nucleus exhibit a lower pH than those closer to the ruffling edge of the cell. The present image processing system is analyzed for linearity of detection, light scattering artifacts, signal to noise ratio, standard curves, and spatial resolution. The results obtained from digital image analysis are shown to be comparable to the results from standard microspectrofluorometry. We also discuss several other applications of this ratio imaging technique in cell biology.

During the past few years, video imaging technology has enabled biologists to acquire information never before obtainable with a light microscope. Studies of morphological changes (8, 19, 20, 44) and analyses of movement (3, 19, 20) have been improved by video microscopy. Weakly luminescent specimens and low light level fluorescence microscopy have necessitated the use of image intensification procedures to record the images in real time (14, 36, 39, 46–49, 52, 54).

Computer processing of digital images from light microscopy has been practiced for at least 15 years (25), although the potential has only been fully realized in the last few years. There now exists a well developed repertoire of image processing algorithms and software packages for image enhancement (i.e., weak images), image restoration (i.e., de-focused images) (42), and pattern recognition (i.e., automatic cell counting and chromosome karyotyping [6, 33–35]). Video processing has recently been used to enhance the contrast, quality, and speed of polarization-based microscopy (2–4, 20) as well as to quantify local fluorescence intensities (22). Digital

image subtraction, a method used in electron microscopy (25, 26), has also been applied to light microscopy (2). Finally, image processing has been proposed as a valuable tool for spectroscopic analyses of cells (38, 40, 53).

It is now apparent that pH plays important roles in various cellular activities (see references 18 and 30 for reviews). A variety of techniques have been described which measure intracellular pH, each having advantages and limitations (29). The two most specific methods for single living cells are micro pH electrodes and fluorescent pH indicators (31, 32). Fluorescent indicators provide good spatial and temporal resolution (15, 16, 50, 51), they can be used with motile cells (15), and can be applied to cell populations (27, 31).

Our laboratory has used the fluorescein fluorescence excitation ratio method (31) to measure pH in single, living cells (15–18, 24). This microspectrofluorometric approach has been valuable, but simultaneous measurements from distinct regions of cells could yield valuable spatial information. This paper describes a method of ratio imaging which generates a

“cellular map” of cytoplasmic pH based on the fluorescein fluorescence excitation ratio method. 2- $\mu\text{m}$  spatial resolution is now possible. The same principle of ratio imaging can also be used to quantify the distribution of specific proteins, to map the concentration of various messengers, and to map the interactions between molecules.

## MATERIALS AND METHODS

**Preparation of Cells:** 3T3 cells (ATCC No. CCL92, final passage No. 125–140) were obtained from American Type Culture Collection (Rockwell, MD). They were inoculated at  $1 \times 10^5$  cells/culture into 25-cm<sup>2</sup> flasks containing CDME<sup>1</sup> (90% Dulbecco's modified Eagle's medium, 10% Gibco newborn calf serum [Gibco Laboratories, Grand Island, NY], 50  $\mu\text{g}/\text{ml}$  penicillin-streptomycin, and 0.292 mg/ml L-glutamine, sterilized by filtration through Nalge 0.2- $\mu\text{m}$  filters [Nalge Co., Rochester, NY]). These cells were incubated at 37°C in 5% CO<sub>2</sub>. On the day before each experiment, the cells were plated at  $5 \times 10^4$  per chamber on Lab-Tek tissue culture chamber/slides (VWR Scientific Co., Boston, MA). These growth phase cells were allowed to attach to the slide for 6 to 12 h at 37°C.

**Preparation of Labeled Macromolecules:** Fluorescein-thiocarbonyl (FTC)-ovalbumin (5 mg/ml, dye/protein = 1.85) was prepared as described (16), FTC-bovine serum albumin (BSA) (9 mg/ml, dye/protein = 4.2) was a gift from P. A. Amato of our laboratory. The FTC-BSA and FTC ovalbumin were dialyzed against the injection buffer (2 mM PIPES, 0.2 mM ATP, 0.1 mM MgCl<sub>2</sub>, 0.2 mM DTT, pH 6.9–7.0) and stored frozen at –20°C until used. FITC-dextran (average molecular weight 39,000, dye/glucose residue = 0.006, which is equivalent to dye/dextran = 1.44) was purchased from Sigma Chemical Co. (St. Louis, MO FD-40, lot 28C-0037). An aqueous solution of fluorescein isothiocyanate (FITC)-dextran was made at 4 mg/ml, pH 7.0. Before injection into cells, all of the labeled macromolecules were clarified by centrifugation at 100,000 g for 30 min in an air-driven Ultracentrifuge (Airfuge, Beckman Instruments, Inc., Spinco Div., Palo Alto, CA) operating at 23 psi air pressure. Fluorescent beads (0.2 to 10  $\mu\text{m}$  diameter) were purchased from Polysciences, Inc. (Warrington, PA). The chromium resolution test target (4.35  $\mu\text{m}$  per line pair) was purchased from Melles Griot (Irvine, CA).

**Microinjection of 3T3 Cells:** Microneedles were prepared from Omega-Dot microcapillary tubes and loaded with labeled macromolecules as previously described (5, 16). Microinjection was carried out on a Zeiss inverted research microscope by applying positive back pressure to needles secured in a Leitz electrode holder. The cells were injected in CHDME (DME without bicarbonate but including 10 mM HEPES, 10% Gibco newborn calf serum, 50  $\mu\text{g}/\text{ml}$  Penicillin-Streptomycin, and 0.292 mg/ml L-glutamine). The injection volume was ~5 to 10% of the total cell volume (5). The cells were allowed to equilibrate for 2 to 4 h at 37°C in the culture medium. Only cells that exhibited normal morphology (spread cells) and retained the labeled macromolecules were analyzed. The FITC-dextran was excluded from the cell nucleus and other vesicles observed by phase-contrast microscopy. Some cells were loaded by a new bulk loading technique (McNeil, P., F. Lanni, R. Murphy, and D. Lansing Taylor, manuscript submitted for publication).

**Pinocytosis of FITC-Dextran by 3T3 Cells:** The medium in the Lab-Tek tissue culture chamber/slide containing spread unloaded 3T3 cells was replaced with up to 40 mg/ml 70,000 mol wt FITC-dextran in CDME at 37°C. The cells were incubated at 37°C for up to 1 h and gently rinsed five times with CHDME at 37°C.

**Microspectrofluorometric Measurement of Fluorescence Intensity Ratio:pH:** The fluorescence intensity ratio (E<sub>489</sub>/E<sub>452</sub>) from single cells injected with FTC-BSA or from flat microcapillaries containing FTC-ovalbumin in standard buffer solutions were measured with our microspectrofluorometer as previously described (24). The wavelengths of emission were 520–560 nm.

**Cytoplasmic pH Measurement by Ratio Imaging:** The fluorescence intensity ratios (E<sub>489</sub>/E<sub>452</sub>) from images of single cells injected with FTC-macromolecules or from flat microcapillaries containing the labeled macromolecules were measured with the image processing system as diagrammed in Fig. 1A. This system is a combination of our microspectrofluorometer and a modified Hamamatsu SIT camera-Frame Memory Image Processor (Hama-

matsu Systems, Inc., Waltham, MA). A Zeiss 63 $\times$ Plan-Neofluar water immersion objective (NA = 1.2) was used throughout the experiments. Although the sensitivity of the SIT camera was approximately an order of magnitude less than that of our microspectrofluorometer, the image processing system allowed us to sum or average incoming video frames (over an area of 128  $\times$  128  $\mu\text{m}^2$ ), which resulted in typically 10 to 22 times enhancement in the incoming signal-to-noise (S/N) ratio at the expense of data acquisition speed.

The measurement of pH by ratio imaging was carried out as diagrammed in Fig. 1B. The image quartering feature of the Hamamatsu Frame Memory allowed us to split the display screen into four quadrants and to sum or to average (sliding average) incoming video frames into any quadrant. Furthermore, we arithmetically and logically operated on stored images in two selected quadrants (or operated on a quadrant and a constant), pixel by pixel, and deposited the resulting image into a selected quadrant. After each trial the resulting quadrant contained the ratio: E<sub>489</sub>/E<sub>452</sub> = (Cell image–background image) excited at 489 nm/(Cell image–background image) excited at 452 nm, which is a function of pH. The background measurements were taken on the same slide close to the measured cell. (In other cell systems where the cells may have detectable autofluorescence, the background images may be taken on the target cell before microinjection of the probe into that particular target cell.)

At this point, the images may be photographed or stored on video tape. Spatial statistics may be computed from images taken at individual excitation wavelengths as well as the resulting ratio image. This involves calculations of the arithmetic mean and standard deviation of pixel values in the area of interest. If it is done with capillary filled with labeled protein (in vitro standard) or with cells whose cytoplasmic pH is clamped to a known pH (in vivo standard), then the S/N ratio may be computed. Temporal statistics were also computed to detect any photobleaching. In addition, the absence of photobleaching can be shown by switching the order of excitation; i.e., taking a ratio image with 452-nm excitation before 489-nm excitation and then another image with 489-nm excitation before 452-nm excitation. The error between the two images disappears as photobleaching diminishes. Photobleaching was not detected under the experimental conditions used in this study.

Random “noise” in the area surrounding the cytoplasmic ratio map despite apparently “clean” cytoplasmic ratios. This type of noise originates from dividing random values of E<sub>489</sub> after background subtraction (the numerator), by random values of E<sub>452</sub> after background subtraction (the denominator). This surrounding ratio noise may be suppressed, without altering the cytoplasmic ratio in any way, by applying an upper threshold function of E<sub>489</sub> and a lower threshold function to E<sub>452</sub>, eliminating the remaining random residual intensities before the ratio is taken. In practice, any residual values of E<sub>489</sub> (the numerator) is cleared to zero intensity while any residual values of E<sub>452</sub> (the denominator) is set to an integer such as 1. Thus, after taking the ratio, the surroundings become zero (dark). The choice of the thresholds depends on the intensity of the image signal and of the residual values after background subtraction. When properly performed, this operation does not alter the pixel ratio in the region of interest. Instead, it suppresses the ratio values of the surroundings and aids in identification of cellular structure, the pH of which is being measured.

The excitation filter changer, image acquisition, and subsequent mathematical operations were controlled by a supervising program in the AIM-65 microcomputer. The intensities of the images produced were printed out, pixel by pixel, on a line printer, or they were fed into the AIM-65 microcomputer to obtain image statistics. Selected images were recorded on an NEC  $\frac{3}{4}$  inch cassette video tape (Nippon Electric Co., Ltd., Tokyo, Japan), or photographed from the TV monitor screen with a Nikkormat camera fitted with a 50 line/inch reticle grating (5, 20) and Ilford HP5 film exposed at 400 ASA and developed in Diafine.

**Linearity of the Ratio E<sub>489</sub>/E<sub>452</sub> as a Function of Radial Distance from Optical Axis:** A fluorescently labeled polystyrene microsphere (diameter 10  $\mu\text{m}$ ; Half Bright, Coulter Electronics, Hialeah, FL) was placed at regular intervals, vertically and horizontally, in the field of view. The error of the ratio E<sub>489</sub>/E<sub>452</sub> taken at particular points and on the optical axis was measured and computed. This error was plotted as a function of radial distance from the optical axis (data not shown).

Although the mean error of emission intensity at both excitation wavelengths (E<sub>452</sub> and E<sub>489</sub>) increased with the radial distance from the optical axis, the mean error of the ratio E<sub>489</sub>/E<sub>452</sub> reached a plateau of approximately  $\pm 6\%$  at 90  $\mu\text{m}$  from the optical axis. By keeping the area of measurement within 60  $\mu\text{m}$  in radius from the optical axis (which is ~70% of the field area), the mean error was reduced to  $\pm 3\%$ . This error level corresponded to 0.15 ratio units. At present, this value is comparable to the contribution of statistical and other experimental errors.

**Controls for Light Scattering by Constituents of the Cytoplasm:** A drop of aqueous solution containing  $1.3 \times 10^6$  particles per milliliter of fluorescently labeled polystyrene particles (10  $\mu\text{m}$  Coulter micro-

<sup>1</sup> Abbreviations used in this paper: CDME, see Materials and Methods, Preparation of Cells; CHDME, see Materials and Methods, Microinjection of 3T3 Cells; FITC, fluorescein isothiocyanate; FTC, fluorescein thiocarbonyl; BSA, bovine serum albumin; NA, numerical aperture; S/N ratio, signal-to-noise ratio; DIT, dithiothreitol.

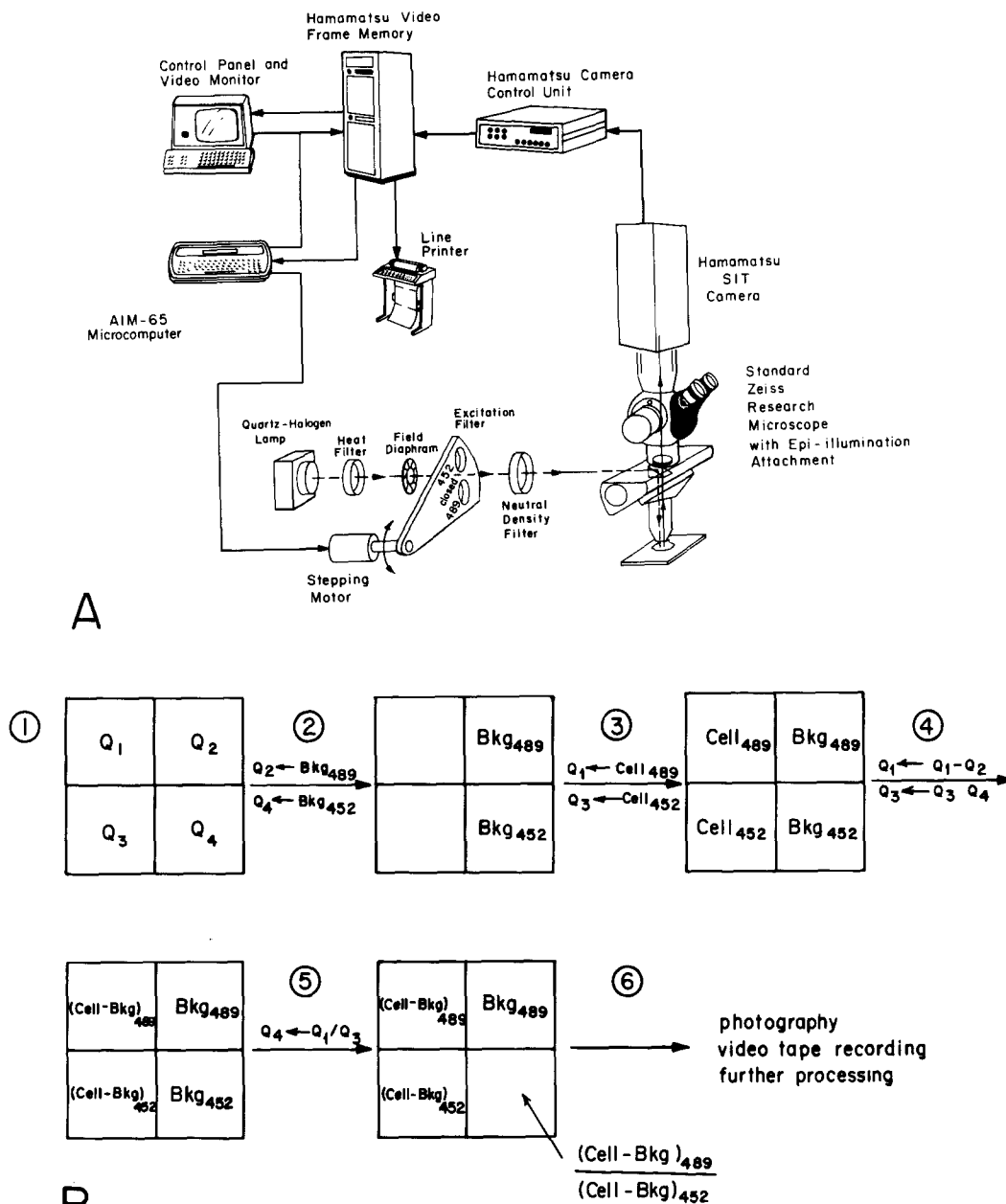


FIGURE 1 (A) Schematic representation of the ratio imaging system. The dashed line represents the epiillumination beam from a quartz-halogen lamp and the heavy solid line represents the path of fluorescent light emitted from the sample. The excitation filter changer is powered by a microprocessor-controlled stepping motor (24). To achieve higher dynamic range and S/N ratio, we mechanically attached a neutral density filter (absorbance = 0.5) (not shown) to the 489-nm excitation filter on the filter changer. Another neutral density filter (transmittance = 25%) is inserted in the excitation path to avoid photobleaching of the probe. The emission beam passes through the 520–560-nm barrier filter in the Zeiss epiillumination assembly to the Hamamatsu SIT camera. The digitized video signal is then processed in the Video Frame Memory and displayed on the video monitor or recorded by a video tape recorder (not shown). The partial and final images may be transmitted to the AIM-65 microcomputer for statistical analysis, or the intensities may be printed out on the line printer for manual analysis. The transmitted-light optics below the specimen stage are not shown for simplicity. (B) Sequence of ratio image acquisition and processing. (1) The modified Hamamatsu Frame Memory System operates in the image quartering mode with its four quadrants labeled Q<sub>1</sub> through Q<sub>4</sub>. (2) Background images at the two excitation wavelengths are stored in quadrants 2 and 4. (3) Fluorescence images of the probe-injected cells excited at the two wavelengths are stored in quadrants 1 and 3. (4) Background subtraction is performed. The subtracted images replace the raw images in quadrants 1 and 3. (5) The threshold function can be applied here to eliminate surrounding residual values and then the ratio can be taken between quadrants 1 and 3. The resulting image is stored in quadrant 4. (The old contents of quadrant 4 are destroyed.) (6) The ratio image can be viewed, recorded, printed, or processed further. The flexibility of the Hamamatsu system allows any different pair of quadrants to be used in addition to the ones shown above.

spheres) was placed in a chamber of a Lab-Tek tissue culture chamber/slide for 30 min to allow the particles to settle. Cells were then plated in the usual manner on the lawn of beads and incubated for 6 h at 37°C. Comparison of the intensity profiles of the fluorescent microspheres that were not covered by

cells and the ones that were covered by cells showed no detectable difference in the intensity profile (excited at 495 nm). The extremely flat 3T3 cells proved to be excellent optical specimens.

Sample Preparation for *In Vitro* pH Standard Curve: The

fluorescence probe concentration was first selected by plotting the ratio E489/E452 as a function of probe concentration. The probe was buffered by 50 mM Tris maleate, pH 7.0, and was sealed in flat microcapillaries (50- $\mu$ m path length, Vitro Dynamics, Rockaway, NJ). This plot gave the range over which the ratio E489/E452 was independent of probe concentration ( $\sim$ 0.5 to 25  $\mu$ M of fluorescein). At higher concentrations, self-quenching and inner-filter effects were detected, while at lower concentrations, the emission intensity was not adequate to produce an acceptable S/N ratio. Our final probe concentration inside the cytoplasm was selected to fall in the optimal range.

Once the concentration of probe was selected, the labeled macromolecules were diluted to the final concentration by 50 mM Tris-maleate buffer, pH 4.0 to 8.0 (18, 24). The solutions were drawn by capillary action into 50  $\mu$ m flat microcapillaries and sealed with paraffin or Valap. These *in vitro* standard curve ratios were measured within 15 min of preparation. Background measurements were performed on capillaries filled with buffer alone.

**Sample Preparation for *In Vivo* pH Standard Curve:** Cells that were measured for "resting" cytoplasmic pH were subsequently incubated in a series of weak acid-base buffers (100 mM ammonium acetate, 10 or 50 mM Tris maleate) ranging from pH 6.13 to 7.00 for 25 min at room temperature. At pH 7.40, the cells were incubated in 30 mM HEPES buffer containing 130 mM KCl and 10  $\mu$ g/ml nigericin for 45 min. Then the ratio E489/E452 was measured as described previously (18, 21, 24). The intensity of selected vertical columns of pixels (one-dimensional sampling) or area (two-dimensional sampling) were displayed on the video monitor screen, printed on the line printer, or transferred to the AIM-65 computer for statistical analyses.

## RESULTS

### Performance of the Ratio Imaging System

The present system takes 8.85 s to record a pair of fluorescent images at two excitation wavelengths with at least 16 decibels (db) spatial S/N amplitude ratio (with background subtraction) as opposed to 1.50 s to obtain a fluorescence

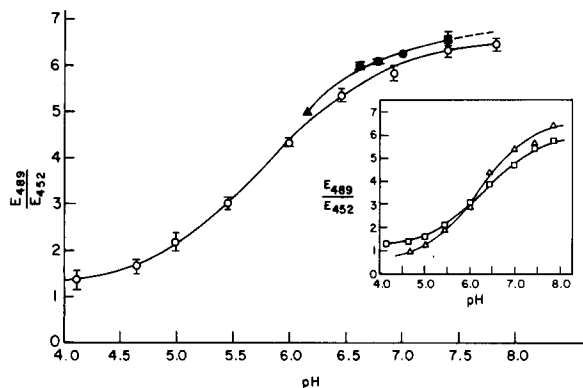


FIGURE 2 pH calibration curve of FITC-dextran. Empty circles: *in vitro* calibration curve made from 0.3 mg/ml FD-40 FITC-dextran in 50 mM Tris-maleate buffer in microcapillaries with 50  $\mu$ m path length. Here the neutral density filter (absorbance = 0.5) was left out to illustrate the effect on standard deviation. Filled circles: several *in vivo* calibration points. Aqueous solution of FITC-dextran was microinjected into 3T3 cells to a final concentration of  $\sim$ 0.3 mg/ml. Both measurements were made on the ratio imaging system. Filled triangles: *in vivo* calibration point obtained from scrape loaded cells in 50 mM Tris maleate, 100 mM ammonium acetate, pH 6.13. Filled squares: *in vivo* calibration point obtained from loaded cells in 30 mM HEPES, 130 mM KCl, 10  $\mu$ g/ml nigericin, pH 7.40. Data for filled symbols were obtained when the neutral density filter was in place and the standard deviation was lowered. Dashed line on *in vivo* standard curve represents extrapolation beyond pH 7.4 based on *in vitro* data. (Inset) Comparison of FITC-ovalbumin *in vitro* pH calibration curves using our microspectrofluorometer (square) and the ratio imaging system (triangle). Each pair of symbols represents measurements done on the same area of the microcapillary tube with 50- $\mu$ m path length. The Hamamatsu Frame Memory is programmed to sum each raw image for 256 frames to improve the S/N ratio.

photon count with 21 db S/N ratio and background subtraction on our microspectrofluorometer. The spatial and temporal S/N ratios may be roughly compared if we assume a normal distribution for both spatial and temporal noise, which can be shown to be the case. For relatively bright cells, the spatial S/N ratio may be between 38 and 48 db (16 db S/N ratio corresponds to error of  $\sim$ 0.10 pH unit, 38 db S/N ratio corresponds to error of  $\sim$ 0.08 pH unit, 48 db S/N ratio corresponds to error of  $\sim$ 0.03 pH units). We also determined the same S/N ratios from experiments performed with a standard test target and a variable illumination source (data not shown).

Each pixel covers the area of  $1.0 \times 1.0 \mu$ m using the 63 $\times$  objective. For relatively dim cells (emission intensity approximately 100 times human visual threshold), the spatial resolution is 4  $\mu$ m or better as determined by the standard test target and by the ability to resolve individual fluorescent beads from fluorescent bead dimers. For relatively bright cells (emission intensity approximately twice that of relatively dim cells), the spatial resolution approaches 2  $\mu$ m for the S/N ratio quoted above. At this stage of development, the pH resolution is 0.20 pH units based on the 0.10 pH unit error in relatively dim cells with 95% confidence. For relatively bright cells, this confidence increases to virtually 100%. These figures are valid within a 20- $\mu$ m diameter region centered on the optical axis. Within a 120- $\mu$ m diameter region, due to imperfect spatial linearity of the system discussed earlier, the confidence is reduced to 58% for dim cells and 73% for bright cells.

### Comparison between Our Microspectrofluorometer and the Ratio Imaging Technique

Fig. 2 (inset) shows the comparison of the *in vitro* standard curves obtained from buffered FITC-ovalbumin in the flat microcapillaries using the two techniques. Although each of the two pH standard curves is distinct, both of them exhibit the same S-shape and are consistent and reproducible. The calibration curve of the ratio imaging technique has a slightly higher slope in the pH range between 6 and 7. Similar comparisons of pH calibration curves (not shown) have been obtained using a Zeiss 25 $\times$  Pol-Neofluar (NA = 0.60) objective instead of the 63 $\times$  Plan-Neofluar (NA = 1.2). The "resting" cytoplasmic ratios in living cells obtained from the two techniques are very close to each other.

Fig. 2 shows the *in vitro* pH standard curve for FITC-dextran and relevant *in vivo* (cytoplasmic) pH standard points obtained by clamping the cytoplasmic pH to a known value with a weak acid-base buffer. The *in vivo* curve exhibits a slightly upward translation from the *in vitro* curve as observed previously (16).

*In vivo* comparison of "resting" cytoplasmic ratio E489/E452 of the same single spread 3T3 cells have been performed using the microspectrofluorometer and the image processing system. FITC-BSA solution, instead of FITC-ovalbumin, was injected into 3T3 cells because of nuclear exclusion that increases the S/N ratio. The microspectrofluorometer covers a spot of 16.9  $\mu$ m diameter (area = 225  $\mu$ m<sup>2</sup>) while ratios within  $15 \times 15 \mu$ m<sup>2</sup> are averaged to give a single value for the image processing system. Ten measurements on the same cell are averaged temporally with the microspectrofluorometer, while 225 pixel ratios (i.e.,  $15 \times 15 \mu$ m<sup>2</sup>) are averaged spatially for the ratio imaging technique. From the three cells mea-

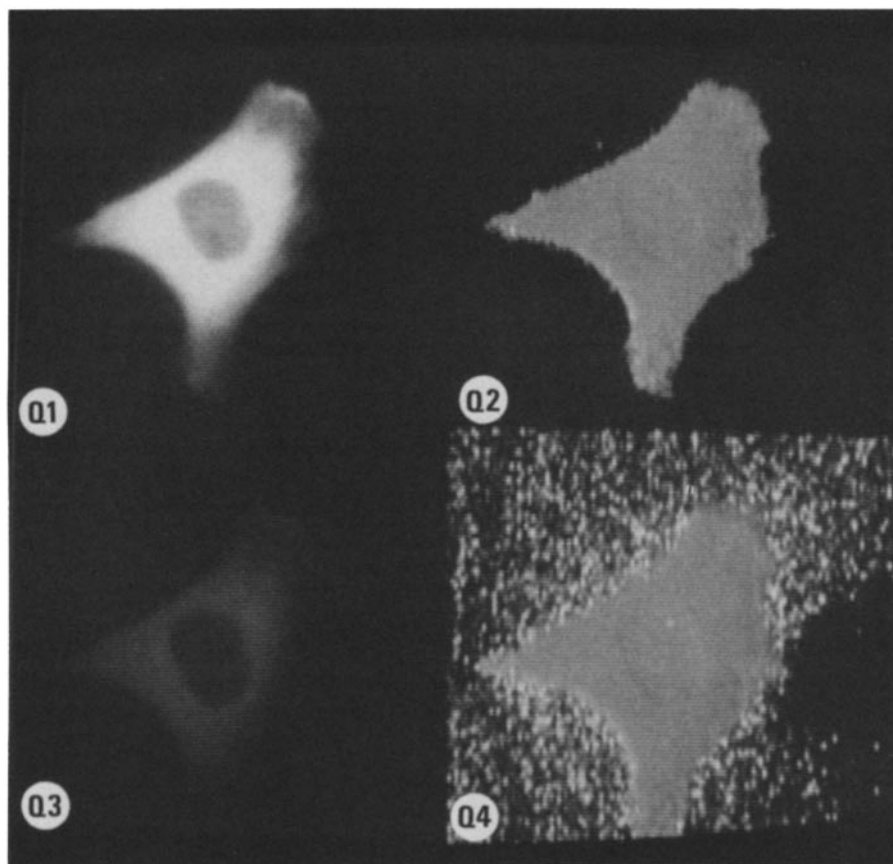


FIGURE 3 An example of the sequence of image processing steps performed by the modified Hamamatsu System (refer to Fig. 1b). Quadrant 1 shows the image formed at 489-nm excitation after background subtraction. Quadrant 3 shows the image formed at 452-nm excitation after background subtraction. Quadrant 4 is a display of the ratio image without the threshold operation to limit the residual background values. Quadrant 2 shows the ratio image after the threshold operation. The spacing between two adjacent raster lines is  $1.0 \mu\text{m}$ .

sured, the microspectrofluorometer gave a mean E489/E452 ratio of  $4.75 \pm 0.15$ , while the image processing system yielded a value of  $4.89 \pm 0.05$ . The slight difference between the two arithmetic means is consistent with the slightly different calibration curves for FITC-BSA in these two systems (data not shown).

### Resting Cytoplasmic pH in 3T3 Cells

Fig. 3 shows the fluorescent images of FITC-dextran in the cytoplasm of a "resting" 3T3 cell. A resting cell is operationally defined as a cell not experimentally stimulated by any agent. The ratio of the two images is taken pixel by pixel to obtain the ratio map. The cells show apparently uniform fluorescence in the cytoplasm with no punctate spots or vesicles. Various organelles, especially the nucleus, exclude FITC-dextran and therefore appear as somewhat dark spots in the bright images. The final ratio, however, shows quite a uniform distribution of the "resting" cytoplasm and in the perinuclear region. We have not detected any significant difference between the cytoplasmic pH near the two ends of these resting cells.

Fig. 4 is a histogram of the average resting cytoplasmic ratio E489/E452 of 3T3 cells microinjected with FITC-dextran. The average pH of all cells is  $6.83 \pm 0.38$ . The distribution seems to be skewed, and non-unimodal. Within the first peak of distribution, the mean pH is calculated to be  $6.74 \pm 0.23$ .

### Pinocytosis of FITC-dextran by 3T3 Cells

Fig. 5 shows the pH map of FITC-dextran-containing pinosomes in 3T3 cells. Pinosomes near the periphery of the nucleus were as much as 0.7 pH unit more acidic than pinosomes in the ruffled cell periphery.

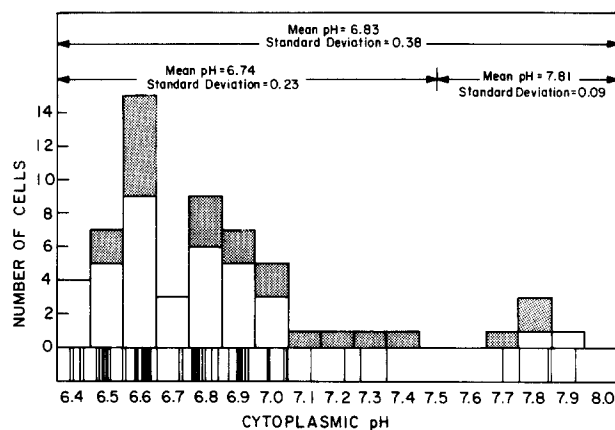


FIGURE 4 Distribution of cytoplasmic pH in single living 3T3 cells. 22 cells were injected with 4 mg/ml FD-40 FITC-dextran to a final concentration of  $\sim 0.3 \text{ mg/ml}$  (shaded bars) while 37 cells were loaded by a bulk loading procedure (McNeil, P., F. Lanni, R. Murphy, and D. Lansing Taylor, manuscript submitted for publication) (white bar). The lines beneath the histogram show the individual data points on the pH scale. The area of measurement in each cell was  $\sim 70\%$  of the cytoplasmic area.

## DISCUSSION

### pH Measurements by Digital Image Processing of Fluorescence Images

The fluorescence ratio method is based on the pH sensitivity of the excitation spectrum of fluorescein (31). It is of value in both microspectrofluorometric (18) and flow cytometric analyses (27) of cells. One advantage of this method is that the ratio not only indicates pH, but also normalizes the data for

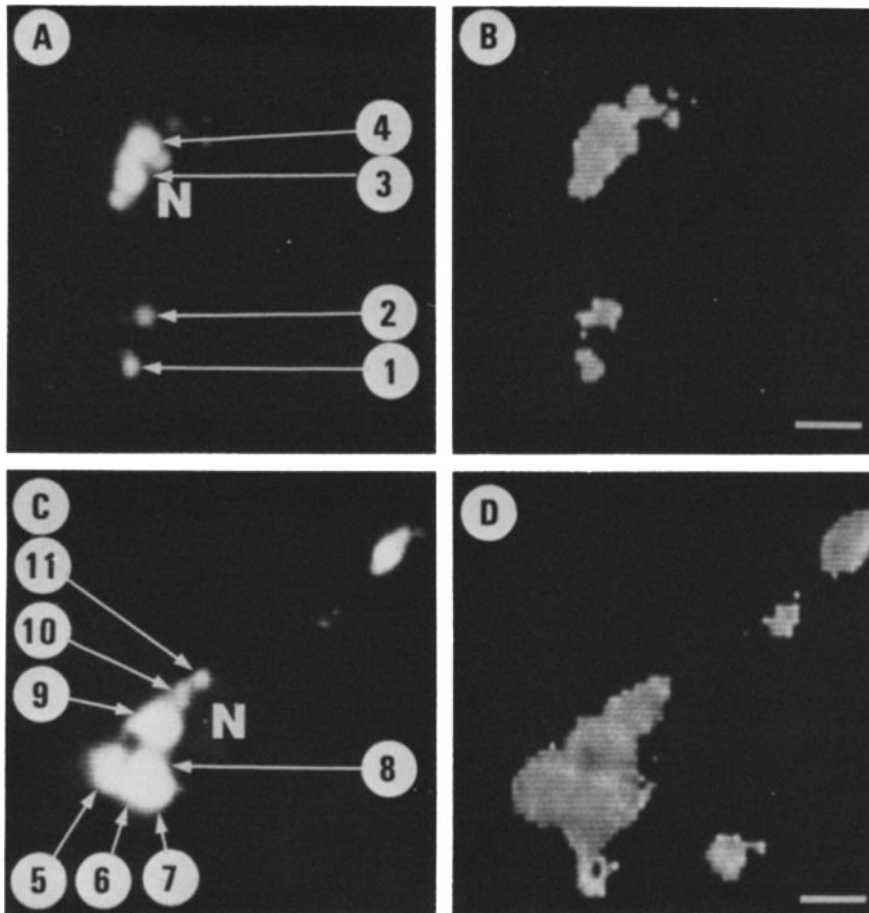


FIGURE 5 pH maps of pinosomes containing 70,000-mol-wt FITC-dextran in 3T3 cells. (A and B)  $E_{489}$  image and ratio image of cell 1; (C and D)  $E_{489}$  image and ratio image of cell No. 2. Cell 1 was incubated for 20 min at 37°C in CDME, pH 7.25, containing 40 mg/ml FD-70 dextran. After rinses of CHDME at 37°C, the cell was incubated in CHDME, pH 7.4, for 10 min before observation. Cell 2 was incubated for 60 min at 37°C in CDME, pH 7.25, containing 40 mg/ml FD-70 dextran. The cell was then rinsed and incubated exactly as cell A. Pinosome images in A and C appear smaller than the corresponding ratio images in B and D because A and C display only the topmost 8 out of 16 possible binary bits in order to show clearly the positions of pinosomes. Pinosome 1 is at the periphery of cell 1 and pinosomes 5, 6, and 7 are at the periphery of cell 2. Pinosomes 2 and 3 in cell 1 have a ratio difference of 0.42 units while pinosomes 5 and 11 in cell 2 have a ratio difference of 0.34 units which are significant since the noise for the ratio is only 0.10 units. (The cells were positioned so that the optical axis is half-way between the nucleus and the cell periphery to minimize spatial nonlinearity of the field.) In general, pinosomes that are closer to the nucleus exhibit lower ratios than the ones farther away; i.e., near the edge of the cells. If we assume that the cytoplasmic standard curve is also applicable to pinosomes, the pinosomal pH will be as follows: (1) 7.10, (2) 7.27, (3) 6.69, (4) 6.87, (5) 6.65, (6) 6.57, (7) 6.61, (8) 6.60, (9) 6.49, (10) 6.45, (11) 6.42. Bar, 10  $\mu$ m.

path length and accessible volume (15, 16). The present results indicate that pH measurements can be made on whole cells with a spatial resolution of at least 2  $\mu$ m using digital image processing on whole cells. Therefore, spatial information can be gained during a variety of cellular processes. The validity of this approach has been demonstrated by comparing results of our microspectrofluorometer (24) with the image processing system (Fig. 2).

We have considered the potential problems of detector linearity, detector sensitivity, probe concentration, and light scattering (see Materials and Methods). Although important technical improvements will be possible, this approach appears to be valid. Future advances will include the following: better temporal and spatial resolution, which will involve the use of more sensitive detectors than the SIT camera; improved statistical analyses and enhancement procedures, which will include interfacing the Hamamatsu Video Frame Memory to a VAX 11/750 computer; and improved graphics with the use of pseudocolor generation. We will also approach the questions of depth of field (in thick specimens), the limit of acceptable light scattering, and improved statistics with matched interference filters.

The ratio imaging technique is the method of choice for single cell analyses. Data from whole cells are collected with a time resolution limited only by the integration time required at each wavelength to obtain an acceptable S/N ratio. Once

the data are stored, the local processor can be used to analyze different regions of the cell using a spatial resolution from that of the whole cell down to the resolution limit (2  $\mu$ m for the present configuration). A "map" of pH in living cells is therefore generated by this method. The full value of this approach will be realized in studies of cellular dynamics such as cell division, cell movement, and responses to a variety of stimuli where both temporal and spatial changes in pH would be expected to occur.

#### Significance of Cytoplasmic pH Results

We report an average resting pH of 3T3 cells of  $6.83 \pm 0.38$ . The standard deviation of pH values within distinct regions of single bright cells is less than  $\pm 0.05$ . The average pH value is close to that reported in other resting mammalian cells. For example, the average resting pH of murine spleen lymphocytes has been reported to be 6.9 (reviewed in reference 10), 7.18 (12, 13), 7.22 (11),  $7.00 \pm 0.05$  (41), and 6.90 to 6.95 (41). The cytoplasmic pH of human leucocytes has been reported as being  $7.104 \pm 0.115$  (1) and  $7.11 \pm 0.02$  (23). In human lymphocytes, the cytoplasmic pH has been found to be 7.25 (7) and 7.31 (55). Most experiments in this area suffer from the fact that cell populations are used to obtain the average pH and the probes in the popular weak acid-base distribution technique appear to permeate all cellular compartments (43).

The cells under study are not synchronized (10); therefore, the skew or bimodal distribution of cytoplasmic pH could reflect a pH change during the cell cycle. An equally possible explanation is some kind of uncharacterized activation of some of these cells by a presently unknown agent, as has been described in the concanavalin A-stimulated murine spleen lymphocytes (11). It is of interest to point out that the distribution of the average cytoplasmic pH of single amoebae, a nonmammalian species, has also been found to be at least bimodal (16). The possible relation between cytoplasmic pH and cell cycle is now under investigation.

### Pinosomal pH

3T3 cells containing pinosomes are ideal specimens for demonstrating the spatial information possible with our digital ratio imaging technique. The size of these pinosomes ranges from below to above the spatial resolution limit of the present system. Besides, the endosomal pH has been shown to drop rapidly in 3T3 and other cell types (17, 24, 27, 28, 45, 51). Fig. 5 shows the pH maps of pinosomes in two 3T3 cells. It is clear that there is an initial drop in pH from the FITC-dextran medium down to the values indicated. At each instance within a given cell, the pH of the vesicles that have traveled to the perinuclear region are lower than that of the vesicles located closer to the cell periphery. Other data show that the pH of pinosomes in the tail cortex of amoebae was higher than that of the pinosomes released into the endoplasm (24). More detailed studies of acidification of a variety of endosomes are now in progress.

### Other Applications of Ratio Image Fluorescence Spectroscopy in the Microscope

The basic concept of ratio imaging is not limited to pH measurements, but can be applied to other fluorescence spectroscopic measurements with the microscope. The ratio method will yield a cellular profile or map of a variety of parameters normalized for path length and accessible volume. Fluorescent indicators of other physiological parameters could be excited at two wavelengths to produce a ratio value related to the concentration. Steady state fluorescence polarization measurements could be made on whole cells by generating a ratio image from sequential images obtained with orthogonal states of polarization. This would produce a cellular map of polarization.

At least two other types of measurements could be made after spectral corrections of the detector. A cellular map of the local concentration of specific fluorescent analogues could be made relative to a control protein using a combination of fluorescent analog cytochemistry (53) and the ratio imaging technique. The ratio of the fluorescent analog and the soluble control protein labeled with a distinct fluorophore yields a cellular map of the relative concentration of the analogue normalized for path length and accessible volume (48, 49, 53). In addition, resonance energy transfer between suitably labeled molecules could be detected by obtaining a ratio of emission intensities of the acceptor and the donor (9, 47).

Fluorescence spectroscopy by digital image processing should yield important spatial and temporal information in living cells during normal cell functions.

It is a pleasure to acknowledge valuable conversations with Drs. R. D. Allen, S. Inoué, E. D. Salmon, E. Haas, A. Waggoner, F. Lanni,

and R. Murphy. Special thanks to the Hamamatsu Corporation for agreeing to work with us on the design and construction of the ratio imaging mode for their image processing system. Mr. Maldari, Mr. Ida, Mr. King, Mr. Kamiya and Ms. Yilmaz helped to make this interaction pleasant and rewarding. Dr. J. Heiple continues to supply us with the wisdom accumulated from her research in quantitative fluorescence measurements. We also appreciate the advice and assistance of members of our laboratory including P. Amato, K. Luby-Phelps, and M. B. Pope.

This work was supported by National Science foundation (NSF) grant PCM-8209017 to D. L. Taylor and G. T. Reynolds, Tobacco Council grant 1412R1 to D. L. Taylor, NSF grant PCM-8119187 to D. L. Taylor, and Department of Energy Contract EY-76-5-02-3120 to G. T. Reynolds.

Received for publication 13 June 1983, and in revised form 14 November 1983.

### REFERENCES

- Ahmed, S., and D. Baron. 1971. Intracellular pH measured in isolated human leucocytes. *Clin. Sci.* 40:487.
- Allen, R. D., and N. S. Allen. 1983. Video-enhanced microscopy with a computer Frame Memory. *J. Microsc.* 129:3-17.
- Allen, R. D., N. S. Allen, and J. L. Travis. 1981. Video-enhanced contrast, differential interference contrast (AVEC-DIC) microscopy: a new method capable of analyzing microtubule-related motility in the reticulopodial network of *Allogromia laticollaris*. *Cell Motility*. 1:291.
- Allen, R. D., J. L. Travis, N. S. Allen, and H. Yilmaz. 1981. Video-enhanced contrast polarization (AVEC-POL) microscopy: a new method applied to the detection of birefringence in the motile reticulopodial network of *Allogromia laticollaris*. *Cell Motility*. 1:175.
- Amato, P. A., E. R. Unanue, and D. L. Taylor. 1983. Distribution of actin in spreading macrophage: a comparative study on living and fixed cells. *J. Cell Biol.* 96:750-761.
- Andrews, H. C., A. G. Tescher, and R. P. Kruger. 1972. Image processing by digital computer. Image restoration and enhancement can be implemented by means of large-scale digital computers, with striking results. *IEEE (Inst. Electr. Electron. Eng.)* 1972(July):21-33.
- Deutsch, C. J., A. Holian, S. K. Holian, R. P. Daniele, and D. F. Wilson. 1979. Transmembrane electrical and pH gradients across human erythrocytes and human peripheral lymphocytes. *J. Cell. Physiol.* 99:79-94.
- Dvorak, J. A., L. H. Miller, W. C. Whitehouse, and T. Shiroishi. 1975. Invasion of erythrocytes by malaria merozoites. *Science (Wash. DC)*. 187:748-750.
- Fernandez, S., and R. Berlin. 1976. Cell surface distribution of lectin receptors determined by resonance energy transfer. *Nature (Lond.)*. 264:411-415.
- Gerson, D. F. 1978. Intracellular pH and the mitotic cycle in *Physarum* and mammalian cells. In *Cell Cycle Regulation*. Academic Press, Inc., New York. 105-131.
- Gerson, D. F. 1982. Determination of intracellular pH changes in lymphocytes with 4-methylumbelliferone by flow microfluorometry. In *Intracellular pH: Its Measurement, Regulation, and Utilization in Cellular Functions*. R. Nuccitelli and D. W. Deamer, editors. Alan R. Liss, Inc., New York. 125-133.
- Gerson, D. F. 1982. The relation between intracellular pH and DNA synthesis rate in proliferating lymphocytes. In *Intracellular pH: Its Measurement, Regulation, and Utilization in Cellular Functions*. R. Nuccitelli and D. W. Deamer, editors. Alan R. Liss, Inc., New York. 375-383.
- Gerson, D. F., H. Kiefer, and W. Eufe. 1982. Intracellular pH of mitogenic-stimulated lymphocytes. *Science (Wash. DC)* 216:1009-1010.
- Gilkey, J. C., L. F. Jaffe, E. B. Ridgeway, and G. T. Reynolds. 1978. A free calcium wave traverses the activating egg of the medaka, *Oryzias latipes*. *J. Cell Biol.* 76:448-466.
- Heiple, J. M. 1981. Intracellular pH in single living cells. PhD Thesis. Harvard University.
- Heiple, J. M., and D. L. Taylor. 1980. Intracellular pH in single motile cells. *J. Cell Biol.* 86:885-890.
- Heiple, J. M., and D. L. Taylor. 1982. pH changes in pinosomes and phagosomes in the amoeba, *Chaetos carolinensis*. *J. Cell Biol.* 94:143-149.
- Heiple, J. M., and D. L. Taylor. 1982. An optical technique for measurement of intracellular pH in single living cells. In *Intracellular pH: Its Measurement, Regulation, and Utilization in Cellular Functions*. R. Nuccitelli and D. W. Deamer, editors. Alan R. Liss, Inc., New York. 22-54.
- Hotani, H. 1979. Micro-video study of moving bacterial flagellar filaments. *J. Mol. Biol.* 129:305-318.
- Inoué, S. 1981. Video image processing greatly enhances contrast, quality, and speed in polarization-based microscopy. *J. Cell Biol.* 89:346-356.
- Jacob, M. H. 1940. Some aspects of cell permeability to weak electrolytes. *Cold Spring Harbor Symp. Quant. Biol.* 8:30-39.
- Koppel, D., M. Oliver, and R. Berlin. 1982. Surface functions during mitosis. III. Quantitative analysis of ligand-receptor movement into the cleavage furrow: diffusion vs. flow. *J. Cell Biol.* 93:950-960.
- Levin, G., P. Collinson, and D. Baron. 1976. The intracellular pH of human leucocytes in response to acid-base change in vitro. *Clin. Sci. Mol. Med.* 50:293.
- McNeil, P. L., L. Tanasugarn, J. Meigs, and D. L. Taylor. 1983. Acidification of phagosomes is initiated before lysosomal enzyme activity is detected. *J. Cell Biol.* 97:692-702.
- Mendelsohn, M. L., B. H. Mayall, and J. M. S. Prewitt. 1968. Digital transformation and computer analysis of microscopic images. *Adv. Optic. Elect. Microsc.* 2:77.
- Misell, D. L. 1978. Image analysis, enhancement and interpretation. In *practical Methods in Electron Microscopy*. A. M. Glauert, editor. North-Holland Publishing Co., Amsterdam. 7:247-254.

27. Murphy, R., E. D. Jorgensen, and C. Canter. 1982. Kinetics of histone endocytosis in Chinese hamster ovary cells. A flow cytofluorometric analysis. *J. Biol. Chem.* 257:1695-1701.
28. Murphy, R. F., S. Powers, M. Verderame, C. R. Cantor, and R. Pollack. 1982. Flow cytometric analysis of insulin binding and internalization by Swiss 3T3 cells. *Cytometry.* 2(6):402-406.
29. Nuccitelli, R. 1982. Intracellular pH measurement techniques: their advantages and limitations. In *Intracellular pH: Its Measurement, Regulation, and Utilization in Cellular Functions.* R. Nuccitelli and D. W. Deamer, editors. Alan R. Liss, Inc., New York. 161-169.
30. Nuccitelli, R., and J. M. Heiple. 1982. Summary of the evidence and discussion concerning the involvement of pHi in the control of cellular functions. In *Intracellular pH: Its Measurement, Regulation, and Utilization in Cellular Functions.* R. Nuccitelli and D. W. Deamer, editors. Alan R. Liss, Inc., New York. 567-586.
31. Ohkuma, S., and B. Poole. 1978. Fluorescence probe measurement of the intralysosomal pH in living cells and the perturbation of pH by various agents. *Proc. Natl. Acad. Sci. USA.* 75:3327-3331.
32. Ohkuma, S., Y. Moriyama, and T. Takano. 1982. Identification and characterization of a proton pump in lysosomes by fluorescein isothiocyanate-dextran fluorescence. *Proc. Natl. Acad. Sci. USA.* 79:2758-2762.
33. Onoe, M., and M. Takagi. 1976. An automated microscope for digital image processing. Part I: Hardware. In *Digital Image Processing of Biomedical Images.* K. Preston, Jr., and M. Onoe, editors. Plenum Press, New York. 17-28.
34. Onoe, M., M. Takagi, and T. Tashiro. 1976. An automated microscope for digital image processing. Part II: Software. In *Digital Image Processing of Biomedical Images.* K. Preston, Jr., and M. Onoe, editors. Plenum Press, New York. 29-46.
35. Preston, K., Jr. 1976. Clinical use of automated microscopes for cell analysis. In *Digital Image Processing of Biomedical Images.* K. Preston, Jr., and M. Onoe, editors. Plenum Press, New York. 47-58.
36. Reynolds, G. T. 1968. Image intensification applied to microscope systems. *Adv. Opt. Elec. Microsc.* 2:1-40.
37. Reynolds, G. T. 1972. Image intensification applied to biological problems. *Q. Rev. Biophys.* 5:295-347.
38. Reynolds, G. T. 1978. Application of photosensitive devices to bioluminescence studies. *Photochem. Photobiol.* 27:405-421.
39. Reynolds, G. T., and D. L. Taylor. 1980. Image intensification applied to light microscopy. *Bioscience.* 30:586-592.
40. Rich, E. S., and J. E. Wampler. 1981. A flexible, computer-controlled video microscope capable of quantitative, spatial, temporal, and spectral measurements. *Clin. Chem.* 27:1558-1568.
41. Rink, T. J., R. Y. Tsien, and T. Pozzan. 1982. Cytoplasmic pH and free  $Mg^{2+}$  in lymphocytes. *J. Cell Biol.* 95:189-196.
42. Robinson, G. S., and W. Frei. 1975. Final Research Report on Computer Processing of ERTS Images. University of Southern California Image Processing Institute Report USCIP1 640.
43. Roos, A., and W. F. Boron. 1981. Intracellular pH. *Physiol. Rev.* 61:296-434.
44. Schatten, H., and G. Schatten. 1980. Surface activity of the egg plasma membrane during sperm incorporation and its cytochalasin B sensitivity. *Dev. Biol.* 78:435-439.
45. Steinman, R. M., I. S. Mellman, W. A. Muller, and Z. A. Cohn. 1983. Endocytosis and the recycling of the plasma membrane. *J. Cell Biol.* 96:1-27.
46. Taylor, D. L., J. R. Blinks, and G. T. Reynolds. 1980. The contractile basis of amoeboid movement. VIII. Aequorin luminescence during amoeboid movement, endocytosis, and capping. *J. Cell Biol.* 86:599-607.
47. Taylor, D. L., J. Reider, J. Spudich, and L. Stryer. 1981. The detection and measurement of actin assembly by fluorescence energy transfer. *J. Cell Biol.* 89:362-367.
48. Taylor, D. L., and Y.-L. Wang. 1980. Fluorescently labelled molecules as probes of the structure and function of living cells. *Nature (Lond.)* 284:405.
49. Taylor, D. L., Y.-L. Wang, and J. M. Heiple. 1980. The contractile basis of amoeboid movement. VII. The distribution of fluorescently labelled actin in living amoeba. *J. Cell Biol.* 86:590-598.
50. Thomas, J. A., P. C. Kolbeck, and T. A. Langworthy. 1982. Spectrophotometric determination of cytoplasmic and mitochondrial pH transitions using trapped pH indicators. In *Intracellular pH: Its Measurement, Regulation and Utilization in Cellular Functions.* R. Nuccitelli and D. W. Deamer, editors. Alan R. Liss, Inc., New York. 105-123.
51. Tycko, B., and F. R. Maxfield. 1982. Rapid acidification of endocytic vesicles containing  $\alpha_2$ -macroglobulin. *Cell.* 28:643-651.
52. Wampler, J. E. 1981. Calibration and optimization of instrumentation for low level bioluminescence measurements. In *Bioluminescence Current Perspectives.* K. H. Neilson, editor. Burgess, Minneapolis, Minnesota. 12-28.
53. Wang, Y.-L., J. M. Heiple, and D. L. Taylor. 1982. Fluorescent analog cytochemistry of contractile proteins. *Methods Cell Biol.* 25(Pt. B):1-11.
54. Willingham, W., and I. Pastan. 1978. The visualization of fluorescent proteins in living cells by video intensification microscopy. *Cell.* 13:501-507.
55. Zieve, P., M. Haghshenas, and J. Krevans. 1967. Intracellular pH of the human lymphocyte. *Am. J. Physiol.* 212:1099.